12th International Symposium on Turbulence and Shear Flow Phenomena (TSFP12)
Osaka, Japan (Online), July 19-22, 2022

# STABILITY AND TRANSITION OF A LAMINAR SEPARATION BUBBLE ON A FINITE WING

**Connor Toppings**
Department of Mechanical and Mechatronics Engineering
University of Waterloo
200 University Avenue W, Waterloo, Ontario, Canada N2L 3G1
ctoppings@uwaterloo.ca

**Serhiy Yarusevych**
Department of Mechanical and Mechatronics Engineering
University of Waterloo
200 University Avenue W, Waterloo, Ontario, Canada N2L 3G1
syarus@uwaterloo.ca

## ABSTRACT

Disturbance amplification in a laminar separation bubble forming on the suction surface of a cantilevered NACA0018 wing at an angle of attack of 6° and Reynolds number of $1.25 \times 10^5$ is studied using a combination of particle image velocimetry measurements and local and non-local linear stability analyses. The experimental measurements reveal the formation of largely two-dimensional roll-up vortices in the separated shear layer at a nearly constant wavenumber and frequency, despite the substantial reduction in the effective angle of attack near the wing tip. The most amplified wavenumber and its growth rate are accurately predicted by linear stability theory outside of the regions of the separation bubble dominated by three-dimensional end effects, with negligible differences between local and non-local stability analyses.

## INTRODUCTION

On lifting surfaces at low chord Reynolds numbers ($Re_c < 5 \times 10^5$), boundary layer transition often occurs downstream of the location of minimum pressure (Carmichael, 1981). If the laminar boundary layer separates, transitions to turbulence, and reattaches, a laminar separation bubble is formed (Tani, 1964). The reduction in stability of the separated laminar shear layer leads to transition through the rapid convective amplification of disturbances (Marxen *et al.*, 2012). Once shear layer perturbations reach substantial magnitudes and non-linear interactions begin, the dominant disturbances evolve into shear layer vortices, which are shed near the location of maximum bubble thickness (Brendel & Mueller, 1988). Three-dimensional deformations of the shear layer vortices eventually cause breakdown to turbulence and the development of a turbulent boundary layer downstream of the LSB (Marxen *et al.*, 2013). Relative to the fully attached flow condition seen when transition occurs prior to separation at higher chord Reynolds numbers, LSB formation reduces lifting surface efficiency (Mueller & DeLaurier, 2003). Because the strength of the adverse pressure gradient strongly influences the location of laminar separation, the stability characteristics of the separated shear layer, and the possibility of reattachment, LSBs are sensitive to changes in the pressure distribution on a wing or turbine blade resulting from changes in angle of attack.

In most practical applications, three-dimensional end effects are present, and the effective angle of attack changes in the spanwise direction. Consequently, changes in LSB transition dynamics may be expected to occur along the span of a wing or turbine blade. In common design analysis methods, such as lifting line theory and blade element momentum theory, spanwise variations are modelled under the assumption that the flow at a given spanwise location is analogous to the flow over a two-dimensional airfoil at an equivalent effective angle of attack. This assumption enables the use of empirical lift and drag data from two-dimensional airfoil tests to predict the performance of practical three-dimensional lifting surfaces. Although numerous studies have considered transition induced by an LSB on two dimensional airfoil or flat plate geometries (e.g., Brendel & Mueller 1988; Watmuff 1999; Marxen *et al.* 2012, 2013), there are few investigations into the transition process on a finite lifting surface. In fact, recent work by the authors suggests that LSB topology on finite lifting surfaces can differ notably from that expected due to effective angle of attack variation along the span (Toppings *et al.*, 2021; Toppings & Yarusevych, 2021). Therefore, the goal of this work is to study stability and transition within an LSB on a finite wing so as to enable more accurate transition prediction methods for situations in which three-dimensional wing or blade tip/root effects are present.

## EXPERIMENTAL SETUP

Experiments were conducted on a rectangular cantilevered NACA 0018 wing model with an aspect ratio of $AR = 2.5$ and a chord length of $c = 0.2\,\mathrm{m}$ at a chord Reynolds number of $Re_c = 1.25 \times 10^5$ and an angle of attack of 6° in the recirculating wind tunnel at the University of Waterloo. The test section has a square $0.6\,\mathrm{m} \times 0.6\,\mathrm{m}$ cross section and a freestream turbulence intensity of less than 0.08%.

To measure the mean three-dimensional velocity field of the LSB on the wing, stereo particle image velocimetry (PIV) was performed in multiple $z$-normal planes along the

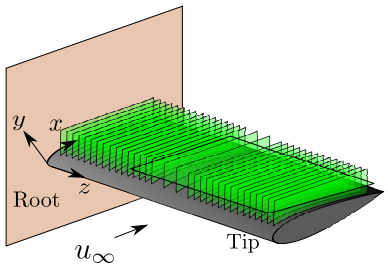


Figure 1: PIV light sheet orientations and surface attached coordinate system definition.

wingspan, termed the side-view configuration, as illustrated in fig. 1 using two LaVision Imager sCMOS 5.5Mpx cameras at a sampling frequency of 52.35 Hz. In addition, two-component time-resolved measurements were performed in planes located at $z/c = 0.95, 1.30, 1.66$ and $2.01$ using two Photron FastCam SA4 1Mpx cameras at a sampling frequency of 3.88 kHz. The flow was seeded with water-glycol fog particles, which were illuminated with a Photonics DM20-527 Nd:YLF pulsed laser and imaged in dual frame mode. Near the wing root and tip, where end effects substantially influence LSB development, the spanwise distance between side-view stereo-PIV planes was $0.05c$.

Another PIV configuration was used to observe the spanwise structure of shear layer vortex shedding in the aft portion of the LSB near the wing tip, where the most significant three-dimensional effects are expected to occur. Two-component PIV using two side-by-side LaVision Imager sCMOS cameras was performed in a single plane tangent to the suction surface of the wing, referred to as the top-view configuration.

Measurements using each PIV configuration were also performed on a nominally two-dimensional NACA 0018 airfoil model as a baseline case. For all PIV measurements, image acquisition and processing were performed using the LaVision DaVis 10 software. Velocity fields were calculated using an iterative multi-pass cross-correlation procedure with a final interrogation window size of 16px $\times$ 16px and 24px $\times$ 24px, resulting in a vector pitch of $5 \times 10^{-4}c$ and $1.9 \times 10^{-3}c$, for the side-view stereo-PIV and top-view configurations, respectively, with 75% overlap between windows.

## STABILITY ANALYSIS METHODS

Previous studies of instability mechanisms in LSBs have shown that the initial stages of disturbance amplification are well-modelled by linear stability theory (e.g., LeBlanc *et al.* 1989; Dovgal *et al.* 1994; Diwan & Ramesh 2009). Linear stability theory assumes that disturbance amplitudes are infinitesimally small so that non-linear interactions between disturbance modes can be neglected (e.g., Herbert & Spalart 1992). The linearised incompressible Navier-Stokes equations govern the evolution of linear disturbances ($\mathbf{q}' = [\mathbf{u}', p']$) in a steady base flow ($\mathbf{U}, P$) (Herbert, 1994):

$$\begin{gathered} \nabla \cdot \mathbf{u}' = 0 \\ \frac{\partial \mathbf{u}'}{\partial t} + \left(\mathbf{u}' \cdot \nabla\right)\mathbf{U} + \left(\mathbf{U} \cdot \nabla\right)\mathbf{u}' = -\frac{1}{\rho}\nabla p' + \nu \nabla^2 \mathbf{u}' \end{gathered} \tag{1}$$

In this study, both local and non-local linear stability analyses are conducted to study the influence of non-parallel effects on the stability characteristics of the separated shear layer of the LSB on the wing model.

In local stability analysis, the base flow is assumed to be parallel, thus $\partial \mathbf{U}/\partial x, \partial \mathbf{P}/\partial x = 0$, and for the case of two-dimensional disturbances, following ansatz is applied to the disturbance modes:

$$\mathbf{q}' = \hat{\mathbf{q}}(y) e^{i(\alpha x - \omega t)} + \text{c.c.} \tag{2}$$

where $\hat{\mathbf{q}}(y)$ is a complex function of only $y$ that describes the mode shape, $\alpha = \alpha_r + i\alpha_i$ is the complex wavenumber, $\omega = \omega_r + i\omega_i$ is the complex frequency, and c.c. is the complex conjugate. When analysing convective instabilities such as those that dominate the transition process in LSBs, $\omega_i$ is assumed to be zero and the disturbance mode is convectively unstable if $\alpha_i < 0$. Local stability analysis does not account for streamwise changes in the base flow or disturbance modes.

In non-local stability analysis, the base flow and the disturbance mode shape functions are allowed to vary slowly in the streamwise direction. By neglecting only the term $\nu \partial^2 \mathbf{u}'/\partial x^2$ in eq. (1), the parabolised stability equations (PSE) are obtained. In non-local stability analysis using the PSE, two-dimensional disturbance modes take the following form:

$$\mathbf{q}' = \hat{\mathbf{q}}(x, y) e^{i\left(\int_{x_0}^{x} \alpha(\xi) d\xi - \omega t\right)} + \text{c.c.} \tag{3}$$

An additional condition is required to partition the streamwise growth between the shape function $\hat{\mathbf{q}}$ and the complex exponential (Herbert, 1994). This is usually done using the condition:

$$\int_0^\infty \hat{\mathbf{q}}^* \cdot \frac{\partial \hat{\mathbf{q}}}{\partial x} dx = 0 \tag{4}$$

where $^*$ denotes complex conjugation. This condition ensures that changes in the energy of the disturbance are contained within $\alpha(x)$, whereas $\hat{\mathbf{q}}(x, y)$ only contains changes to the shape of the mode.

Local and non-local stability calculations were performed using the mean velocity fields at each side-view stereo-PIV measurement plane to explore how the stability characteristics of the separated laminar shear layer vary along the span. To reduce the sensitivity of wall-normal velocity derivatives to experimental noise, the mean velocity fields were preprocessed by applying a smoothing spline fit to the measured velocity profiles at each $x$ location. The linearised Navier-Stokes equation was discretised in the wall-normal direction with a spectral collocation technique using Chebyshev polynomials. For non-local analysis using the PSE, streamwise derivatives of the disturbance modes were evaluated using first order backward differencing, and the solution for $\mathbf{q}'$ was obtained by marching in the streamwise direction. More details of the numerical methods employed in the stability calculations can be found in Westerbeek (2020). Due to the limited extent of the field of view of PIV measurements, calculation of amplification factors (van Ingen, 2008) by integrating $\alpha_i$ starting from the critical point is not possible. Since the most rapid disturbance amplification is expected to occur in the separated shear layer contained entirely within the streamwise extent of the PIV field of view, amplification factors were estimated starting the integration from the upstream end of the PIV field of view. The uncertainty of the linear stability calculations was estimated using a Monte-Carlo method whereby the mean velocity fields were perturbed by normally distributed noise of the same amplitude as the uncertainty in the velocity field measurements.

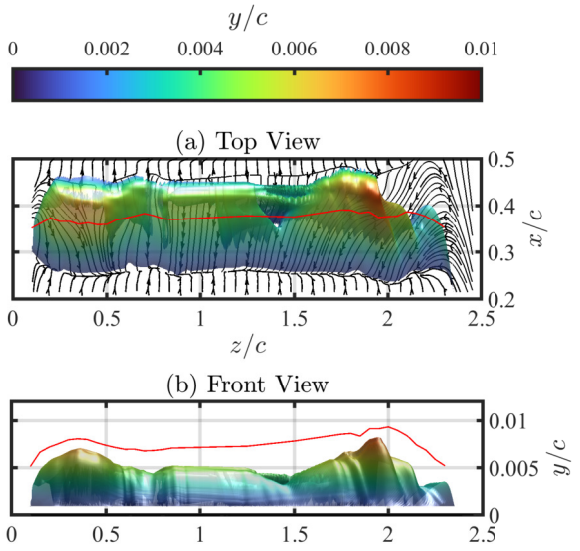


Figure 2: Skin friction lines and streamsurface of separation coloured by wall-normal height. Red line: location of data presented in fig. 5

## RESULTS AND DISCUSSION

The three-dimensional shape of the LSB formed on the suction surface of the wing model is illustrated in fig. 2, which presents skin friction lines calculated from the near-wall velocity gradient and the streamsurface of separation that emanates from the separation line. The topology is that of an open bubble, whereby spanwise flow enters the LSB at the wing root and tip, resulting in a spanwise flow within the LSB near its ends. The colouring of the streamsurface of separation indicates the wall-normal extent of the LSB, revealing that local thickening of the bubble occurs near the wing root and tip where fluid flows into the bubble.

As detailed in Toppings *et al.* (2021) and Toppings & Yarusevych (2021), the LSB forming on the finite wing differs from the LSB forming on the same two-dimensional airfoil section at the same effective angles of attack. In contrast to the downstream shift in LSB location expected due to the substantial reduction in effective angle of attack near the wing tip, the LSB location on the wing remains largely uniform along the span, except in relatively close proximity to the tip. Along the majority of the span, boundary layer separation occurs at $x/c \approx 0.25$, and reattachment at $x/c \approx 0.45$.

The formation and development of coherent structures on the outboard portion of the wing is depicted in fig. 3, which presents instantaneous streamwise velocity contours from the top-view PIV configuration. Because the light sheet for the top-view PIV configuration was positioned to intersect the top halves of the shear layer vortices, the roll-up vortices appear as spanwise bands of increased streamwise velocity. Shear layer roll-up occurs near $x/c \approx 0.40$, and the spanwise uniformity of the vortices for $z/c < 2.15$ suggests that the transition process in a three-dimensional LSB on a wing does not respond to local changes in the effective angle of attack, but that the vortex shedding locks onto a single instability mode across the entire LSB. For $z/c > 2.20$, vortex shedding ceases abruptly, and transition does not occur within the field of view because downwash from the wing tip vortex suppresses boundary layer separation. The high degree of spanwise uniformity in the roll-up vortices is unexpected, since the growth rates and wavenumbers of unstable disturbances are known to be influenced by the distance of the separated shear layer from the wing surface Dovgal *et al.* (1994) which varies substantially in the spanwise direction.

The spanwise and streamwise variations in the frequency of the most unstable disturbance mode in the separated laminar shear layer predicted by local stability analysis are illustrated in fig. 4a, which shows relatively small spanwise variations for $z/c < 2.00$. For $z/c > 2.25$, the most unstable frequency is substantially reduced because the boundary layer remains attached near the wing tip. The expected frequency of the most amplified disturbances on the wing based on the effective angle of attack variation and empirical correlation from time-resolved PIV measurements on the same NACA 0018 two-dimensional airfoil is shown by the dashed line in fig. 4b, with the shaded area representing the experimental uncertainty bounds. The markers indicate the central frequency of the most amplified disturbances on the wing estimated from spectral analysis of time-resolved PIV measurements of wall-normal velocity fluctuations. Whereas a substantial reduction in the most amplified frequency near the wing tip is expected from the two-dimensional airfoil measurements as a result of the reduction in effective angle of attack near the wing tip, the measurements on the wing do not show a corresponding reduction near the wing tip, indicating that the transition process in the LSB does not follow the trend expected from sectional variation of the effective angle of attack along the span. The solid line in fig. 4b indicates the frequency of the disturbance mode with the largest amplification factor at the approximate location of shear layer roll-up ($x/c \approx 0.40$, fig. 3) from local linear stability analysis. On the average, the results follow the trend of the experimentally measured frequencies on the wing. This suggests that spanwise changes in the mean LSB structure on the wing are at least partially responsible for the higher frequency of the most amplified disturbances measured on the wing relative to the two-dimensional airfoil at the same effective angle of attack. Specifically, the local thickening of the LSB near the wing tip (fig. 2) is expected to contribute to the observed increase the most amplified frequency in the outboard portion of the bubble.

Wavelet analysis using the morse wavelet (Olhede & Walden, 2002) was performed to obtain the wavenumbers and growth rates of the most unstable disturbances in the separated shear layer using the wall-normal velocity fluctuation measurements from each side-view stereo-PIV measurement plane. The wavenumber of the most amplified disturbance mode in the separated laminar shear layer is plotted in fig. 5a for the spanwise region within which vortex shedding occurs ($0.10 \leq z/c \leq 2.20$). The data are taken at the streamwise location depicted by the red line in fig. 2, located three-quarters of the streamwise distance from the separation point to the point of maximum LSB height and at $y = \delta_x^*$. This location was chosen so that disturbance amplitudes remain measurable but relatively small ($< 0.05U_\infty$) to ensure that the assumptions of linear stability theory are valid for neglecting non-linear interactions. Within $0.15 < z/c < 2.00$, the most amplified wavenumber obtained using wavelet analysis from the experiment is largely invariant, in agreement with the top-view PIV results (fig. 3). However, a large reduction in the most amplified wavenumber occurs near the wing root at $z/c = 0.10$, and a progressive increase in the most amplified wavenumber is seen in the experimental data near the wing tip ($z/c \geq 1.75$). These changes are attributed to three-dimensional effects near the ends of the LSB. Away from the wing root and tip, the most amplified wavenumbers predicted by local and non-local linear stability maintain a nearly constant value across the LSB. The

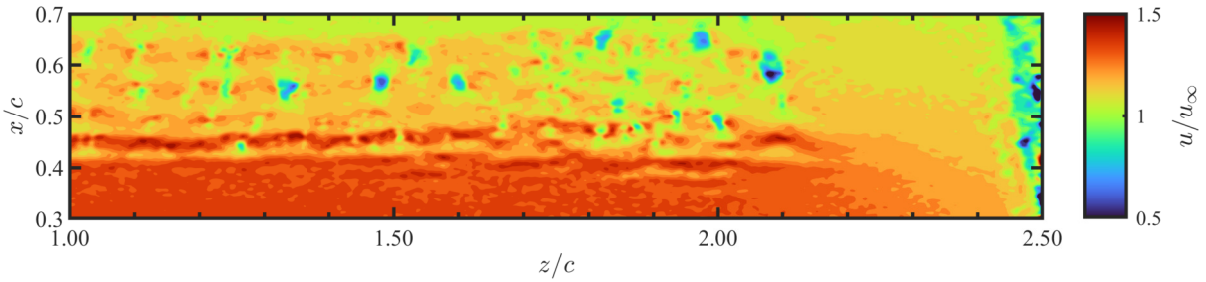


Figure 3: Snapshot of shear layer vortex development in the aft portion of the LSB near the wing tip from top view PIV. Spanwise vortices appear as bands of increased streamwise velocity.

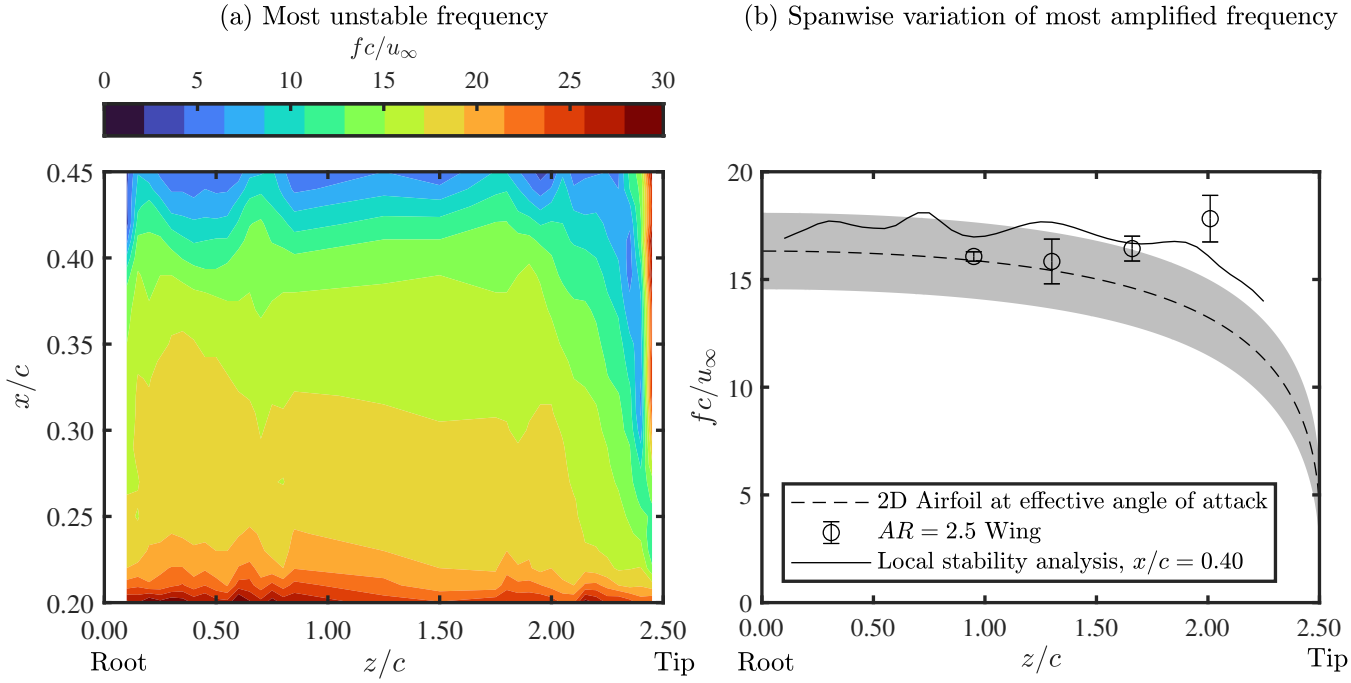


Figure 4: Frequency of most unstable normal disturbance mode calculated from local stability analysis (a), and comparisons of the spanwise variation of the most amplified frequency expected from two-dimensional airfoil measurements, finite aspect ratio wing measurements, and local stability analysis (b).

differences between the most amplified wavenumbers measured in the experiment and those predicted by local and non-local analyses are of similar magnitude as the experimental uncertainty for $0.15 \leq z/c \leq 2.0$, but near the ends of the LSB, the changes in the experimentally measured wavenumber are not well predicted by either local or non-local linear stability analysis. These results suggest that non-parallelism and boundary layer growth do not play a major role in disturbance amplification within the LSB on the finite wing.

The changes in frequency (fig. 4b) and wavenumber (fig. 5a) of the most amplified disturbance mode near the wing tip imply an increase in phase speed. Since fig. 3 shows that the roll-up vortices become progressively weaker for $z/c > 2.10$, the changes in the most amplified frequency and wavenumber near the wing tip are likely the result of slower growth of the primary instability mode in the region influenced by downwash from the wing tip vortex.

In fig. 5b, the growth rates of the most amplified wavenumber at each side-view stereo-PIV measurement location are plotted. Near the wing tip, a substantial reduction in the growth rate occurs where the LSB thickness decreases as a result of downwash from the tip vortex. A relatively smaller reduction in growth rate is also observed near the wing root, where the interaction with junction flow reduces the size of the LSB. The maximum growth rates from local and non-local stability analyses do not show any substantial differences, providing further evidence that non-local effects do not play a major role in the LSB on the finite wing. There is a good agreement between the maximum growth rates of the most amplified wavenumber from the experiment and from linear stability analyses for $z/c \leq 2.00$. Closer to the wing tip, the linear stability analysis tends to over-predict the maximum growth rate of the most amplified wavenumber relative to the experiment, although the differences fall within the expected uncertainty of stability predictions (Boutilier & Yarusevych, 2013).

## CONCLUSION

The LSB forming on the suction surface of a rectangular, cantilevered NACA0018 wing with an aspect ratio of 2.5 was investigated using particle image velocimetry and linear stability analyses at an angle of attack of 6° and a chord Reynolds number of $Re_c = 1.25 \times 10^5$. Except for the regions in the immediate vicinity of the wing root and tip, the locations of sep-

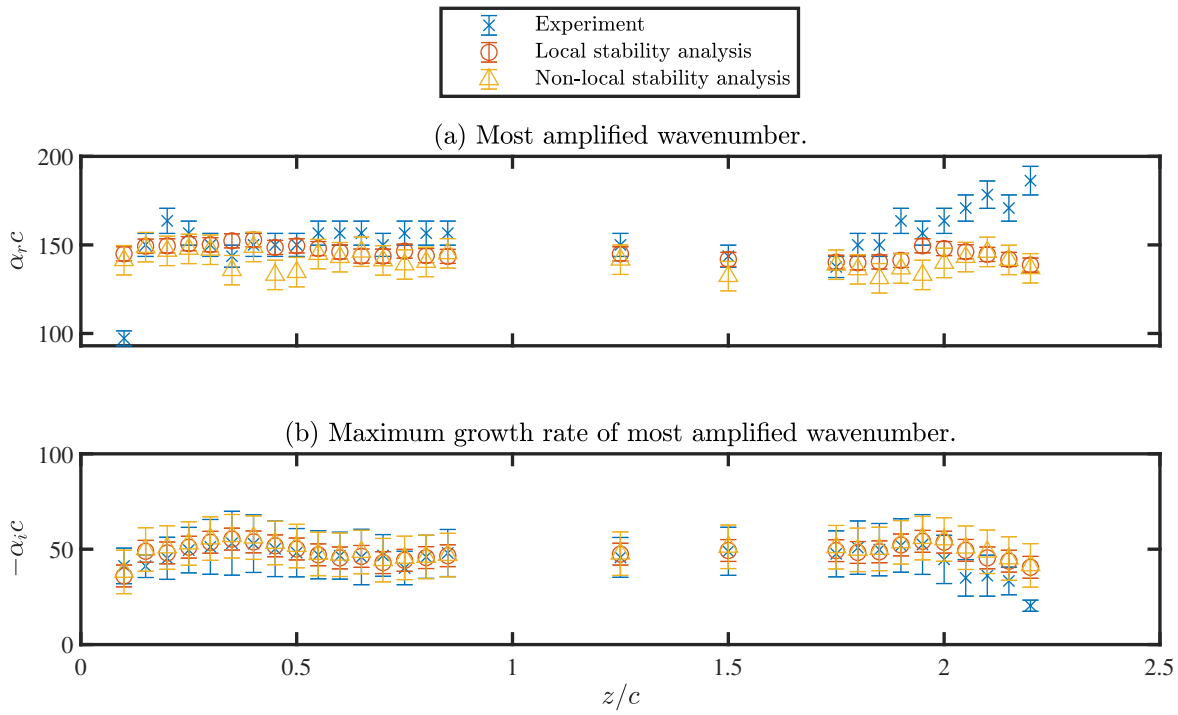


Figure 5: Spanwise variation of most amplified wavenumber (a), and maximum growth rate of most amplified wavenumber (b).

aration and reattachment and the frequencies and wavenumbers of the most amplified disturbances are largely spanwise uniform, despite the significant reduction in effective angle of attack near the wing tip and the spanwise variations in LSB thickness. This leads to the formation of essentially two-dimensional roll-up vortices in the aft portion of the LSB at a nearly spanwise invariant wavenumber in the midspan region of the wing. Near the wing root and tip, the most amplified wavenumber decreases and increases, respectively, but these changes are not accurately predicted by linear stability analysis. However, a reduced growth rate of the most amplified wavenumber in the regions influenced by three-dimensional effects near the wing root and tip is seen in both the experimental measurements and linear stability analysis. The growth rate of the most amplified wavenumber is accurately predicted by local and non-local stability analyses over a majority of the wing span, except for the region within $0.35c$ of the wing tip where linear stability analysis over-predicts the growth rate of the most amplified disturbance mode. The close agreement between local and non-local linear stability analyses leads to the conclusion that non-parallel effects do not significantly influence disturbance amplification in the typical short LSB forming on the finite wing at aspect ratios for which the span sufficiently separates the flow regions affected by the end conditions.

## REFERENCES

Boutilier, Michael S.H. & Yarusevych, Serhiy 2013 Sensitivity of linear stability analysis of measured separated shear layers. *European Journal of Mechanics - B/Fluids* **37**, 129–142.

Brendel, M. & Mueller, Thomas J. 1988 Boundary-layer measurements on an airfoil at low Reynolds numbers. *Journal of Aircraft* **25** (7), 612–617.

Carmichael, B H 1981 Low Reynolds Number Airfoil Survey. *Tech. Rep.* NASA CR-165803. Low Energy Transportation Systems, Capistrano Beach, CA.

Diwan, Sourabh S. & Ramesh, O. N. 2009 On the origin of the inflectional instability of a laminar separation bubble. *Journal of Fluid Mechanics* **629**, 263–298.

Dovgal, A.V., Kozlov, V.V. & Michalke, A. 1994 Laminar boundary layer separation: Instability and associated phenomena. *Progress in Aerospace Sciences* **30** (1), 61–94.

Herbert, Thorwald 1994 Parabolized stability equations. *Tech. Rep.* AGARD Report 793(4).

Herbert, Th & Spalart, P. R. 1992 Linear and nonlinear stability of the blasius boundary layer. *Journal of Fluid Mechanics* **242** (34), 441–474.

van Ingen, J. 2008 The eN Method for Transition Prediction. Historical Review of Work at TU Delft. In *38th Fluid Dynamics Conference and Exhibit*, pp. 1–49. Reston, Virigina: American Institute of Aeronautics and Astronautics.

LeBlanc, P., Blackwelder, R & Liebeck, R 1989 A Comparison Between Boundary Layer Measurements in a Laminar Separation Bubble Flow and Linear Stability Theory Calculations. In *Low Reynolds Number Aerodynamics* (ed. Thomas J. Mueller), pp. 189–205. Berlin, Heidelberg: Springer Berlin Heidelberg.

Marxen, Olaf, Lang, Matthias & Rist, Ulrich 2012 Discrete linear local eigenmodes in a separating laminar boundary layer. *Journal of Fluid Mechanics* **711**, 1–26.

Marxen, Olaf, Lang, Matthias & Rist, Ulrich 2013 Vortex formation and vortex breakup in a laminar separation bubble. *Journal of Fluid Mechanics* **728**, 58–90.

Mueller, Thomas J. & DeLaurier, James D. 2003 Aerodynamics of Small Vehicles. *Annual Review of Fluid Mechanics* **35** (1), 89–111.

Olhede, S.C. & Walden, A.T. 2002 Generalized Morse wavelets. *IEEE Transactions on Signal Processing* **50** (11), 2661–2670.

Tani, Itiro 1964 Low-speed flows involving bubble separa-

tions. *Progress in Aerospace Sciences* **5**, 70–103.

Toppings, Connor E, Kurelek, John William & Yarusevych, Serhiy 2021 Laminar Separation Bubble Development on a Finite Wing. *AIAA Journal* **59** (8), 2855–2867.

Toppings, Connor E. & Yarusevych, Serhiy 2021 Structure and dynamics of a laminar separation bubble near a wingtip. *Journal of Fluid Mechanics* **929**, A39.

Watmuff, Jonathan H. 1999 Evolution of a wave packet into vortex loops in a laminar separation bubble. *Journal of Fluid Mechanics* **397**, 119–169.

Westerbeek, Stephen H.J. 2020 Development of a Nonlinear Parabolized Stability Equation (NPSE) Analysis Tool for Spanwise Invariant Boundary Layers. Master thesis, TU Delft.